Author's response to Review RC1 by Emmanuel Dekemper

We are very grateful for the constructive comments of Emmanuel Dekemper, which led to a very valuable extension of the manuscript. As a major point, we added the retrieval of SO2 CDs from apparent absorbances determined with the prototype instrument, which indicates the possibility of calibration free measurements.

In the following, we will answer the individual comments. For clarity we numbered them from 1) to 6) (bold font). The original reviewer comment is set in italic font, the authors' response in normal font.
We add the two sections (Sect 2.2 and Sect 4) and four Figures (1, 6, 7, 8), containing the major changes to the end of this file.

Specific comments/questions:

1)

It is true that the concept of aligning the transmission comb of the FPI with the periodic structures of the absorption cross-section of species has been described by the author in an earlier paper. However, I would have liked to see a bit more description here as well. For instance, the radiometric model of the measurements described in section 2.2 should make clearer that the measured signals I_A *or* I_B *are made out of photons captured by each transmission peak of the FPI at the same time. Equation (5) could emphasize this by expressing* I *as the result of this summation process. Alternatively, one could bring equation (6) into section 2.2.*

This is a good point. We extended Section 2.2 by a new Equation (Eq. 6), clarifying that I_A and I_B are spectral radiances integrated over the FPI spectral transmission interval. Furthermore, we added Fig. 1c in order to clarify the detection principle and also to visualize the optimisation of the instrument parameters for the individual trace gases (also regarding comment 2a).

2)

a) *Figures 2, 3, and 4 show a possible setting of the FPI targeting a different species respectively. One can imagine that the performance of the measurement method is strongly determined by the capability of finding the best "position" of the FPI comb in order to maximize the correlation. I found that this could have been pointed out and discussed in more details, by showing for instance how evolves this correlation as a function of a spectral displacement of the comb.*

b) *For instance, by looking at figure 4 (NO2), one observes that one of the FPI peaks of the off channel actually captures a relatively high absorption. This sounds like a suboptimal configuration whose impact could have been dealt with.*

a) This point is largely covered by our response to comment 1). The best "position" (d_A and d_B) are also indicated in Fig. 1c, representing the strongest optical density modulation.

b) Indeed the correlation of optimized FPI transmission spectrum and spectral trace gas absorption doesn't look optimal to the eye for the case of NO_2. This is because, the strong absorption band of NO_2 at around 425 to 450 nm are not equidistant. This results in a lower sensitivity, compared for example to a measurement setup where a single FPI transmission

peak is isolated and tuned to maximum and minimum absorption (e.g. at 435nm and 438nm). However, regarding the signal to noise ratio, which is also dependent on the total transmission of the instrument and cross interferences with other gases our proposed setup shows a optimal performance for our boundary conditions. There might be different optimal settings for other scenarios (e.g. a scenario with low NO_2 levels but high scattered sunlight radiances). We added the following explanation to Sect. 3.2:

'The absorption bands of NO_2 are not ideally periodic in the chosen wavelength window. Therefore at first glance they appear to be non-ideal for FPI correlation. The apparent absorbance, however, is still reasonably high with extremely low cross interferences to water vapour and O_4. This demonstrates, that periodical absorption structures are ideal but not necessary for FPI Correlation Spectroscopy. For a different measurement scenario (here we optimised for stack and ship emissions, see above) there might also be a better choice for instrument parameters. For instance for a high radiance and low NO_2 scenario one might use a single FPI transmission peak on the NO_2 absorption band at ~435 nm (as setting A) and at ~438nm (as setting B) in order to increase the sensitivity (see Fig. 4).'

3)

The determination of the CD eventually depends on the knowledge of the effective differential cross-section as shown in eq. (5). However, the way to determine this quantity is not discussed. With the actual instrument, will there be sufficient knowledge of the FPI transmission curve and of the BPF to compute it from a high resolution cross-section dataset? Or will it be necessary to measure it in the lab?

Depending on the knowledge of instrument parameters the instrument function can be modelled and used, together with a simple atmospheric radiation model, to determine CDs from apparent absorbances. We added an explanation to Sect. 2.2 and performed the CD calculation for our prototype data in Sect. 4.2. (see response to comment 4).

4)

The field experiment shows encouraging results, although it does not go up to comparing SCDs retrieved by the FPI-based instrument with the ones obtained from the classical grating-based instrument. As a reader, one immediately wonders why it is like that. Is it because there is no a priori knowledge of the effective differential cross-section (see point before), or because no clear sky measurement could be made at the time of the measurements?

This is a very good comment that led us to calculate SO_2 CDs from the apparent absorbance data, without the use of data provided by the co-aligned DOAS spectrograph. The possibility of calibration free measurements that could be shown to work pretty well for our SO_2 study constitutes another substantial advantage of our FPI-technique.
Section 4 was subdivided into 3 parts: In '4.1 Sensitivity and ozone interference' the proof of concept study is introduced and the correlation of apparent absorbance with DOAS CDs as well as the ozone interference are presented. In '4.2 Calculation of SO_2 CDs by modelling effective absorption cross sections' the model is described and the results of the retrieved FPI CDs are validated with the DOAS data. The outlook to the imaging application is given in '4.3 Imaging'.
In addition to the changes in Section 4, we added the following sentence at the end of the introduction:

'Further, we show that SO_2 CDs can be accurately retrieved from the recorded data without calibration (Sect. 4).'

And we added the explanatory text to the conclusions:

'Further, SO_2 CDs could directly be calculated from the instrument model and a very simple radiative transfer model very accurately and with a ~10% uncertainty of the sensitivity. This indicates that CDs can be retrieved directly from the FPI radiance data without calibration.'

In order to further clarify the measurement, we included the reference (zenith sky) measurement into the time series in Fig. 6. It was taken a few minutes before the plume measurement.
Finally, we removed the dashed grey line labelled with 'simulation' in Fig. 7 and added the result of the FPI CD calculations in an additional Fig. 8.

5)

In the discussion of the results of the field experiment, there is time spent on the interference by O3. However, in absence of any attempt to retrieve the SO2 CD from the FPI-based measurements, it is difficult to adhere to the conclusions of the author about a relative insensitivity to O3. On the other side, if this sensitivity is more robustly confirmed, this aspect is an important asset compared to the widespread SO2 cameras, and emphasized further.

We address this point in our response to comment 4) and by the related changes in the manuscript.

6)

In section 3, there are some inconsistencies between the text and Table 1 which it is referring to. Furthermore, the paragraph is not making it completely clear that the selected CDs are actually detection limits. In particular, for NO2, a value of 1e16 is clearly not the maximum that can be observed above a smokestack, hence it must be a detection limit... This is however better stated in the caption of Table 1.

This is true. We added 'required detection limit of' in the brackets containing the detection limits in the text in Sect. 3. We also corrected the NO_2 CD assumed for stack emission NO_2 cross sensitivities of 1e16 to 1e17 molec cm^{-2} in the text. The simulation was done for 1e17 $molec^{-2}$ (see Tab. 1 and Fig. 2).
We additionally changed the NO_2 CD in the visualisation of the differential optical density in Fig. 4a from 1e17 to 1e16 molec cm^{-2}. That way, all the Figures (Fig. 2, 3, 4) visualise the spectral differential optical density of the target trace gas for the respective target detection limit.

Technical corrections:
- *p.2,L.21: repeated "by column"* corrected as proposed
- *p.2,L.22: replace "rather high" by "rather large" or "rather long"* corrected as proposed
- *p.2,L.27: add a comma after "imaging techniques"* corrected as proposed
- *p.3,L.5: replace "Due to" by "Thanks to"* corrected as proposed
- *p.3,L.11: add commas before and after "for the three gases"* corrected as proposed
- *p.3,L.12: replace "by around" by "about"* corrected as proposed

• *p.4,L.1: remove "a stable"* corrected as proposed
• *p.5,L.28: "calculated" is misspelled* corrected as proposed
• *p.7,L.15: remove the comma after "this illustrates"* corrected
• *p.10,L.6-7: the end of the sentence is very clear.* corrected: removed ‘and’ before ‘trace gases’

We performed the suggested technical corrections.

The following Sections and Figures were revised substantially, mainly due to comment 1, 3) and 4):

2.2 Detection principle

The concept of using FPI correlation to detect atmospheric trace gases is described in Kuhn et al. (2014). The correlation of periodic absorption structures of atmospheric trace gases and the FPI transmission is exploited. An apparent absorbance $\tilde{\tau}_i$ of a trace gas i is calculated from the optical densities of an on-band τ_A and off-band τ_B channel:

$$\tilde{\tau}_i = \tau_A - \tau_B = \log\frac{I_{A,0}}{I_A} - \log\frac{I_{B,0}}{I_B} = (\overline{\sigma}_{A,i} - \overline{\sigma}_{B,i})\, S_i = \Delta\overline{\sigma}_i\, S_i \tag{5}$$

S_i denotes the CD of a trace gas i. For the on-band channel, the spectral pattern of the FPI transmittance is chosen to correlate with the absorption band structure of the target trace gas, while for the off-band channel the FPI is tuned to show minimum correlation with the target trace gas absorption (see Fig. 1). The apparent absorbance is - for low trace gas optical densities - proportional to the CD of the trace gas. The proportionality is $\Delta\overline{\sigma}$, representing the difference of the effective absorption cross section seen by channel A and channel B. The optical densities τ_k are calculated from measured radiances I_k transmitted by the FPI in a setting $k = A, B$:

$$I_k = \int_{\Delta\lambda} I(\lambda) \cdot T_{FPI,k}(\lambda)\, \mathrm{d}\lambda \tag{6}$$

$I_{k,0}$ denotes the reference radiance without the target trace gas in the light path. In practice, a wavelength range $\Delta\lambda$ of high correlation of spectral trace gas absorption and FPI transmission is preselected with a band pass filter (BPF). Within this spectral range the FPI physical parameters are optimised. Figure 1c shows the optical density of BrO seen through an FPI with varying surface displacement d. The maximum difference between maximum and minimum optical density determine the FPI settings A and B. In addition, the Finesse is chosen to maximise the signal to noise ratio.

Here we apply FPI Correlation Spectroscopy for passive imaging of a trace gas in the atmosphere. This means that the light source is scattered sky radiation that is measured within an imaging FOV (e.g. 20° aperture angle). We assume in the following that a reference I_0 (i.e. a part without trace gas) is always present within the image, so that S denotes the differential trace gas CD compared to that reference.

The proportionality $\Delta\overline{\sigma}$ of apparent absorbance $\tilde{\tau}$ and trace gas CD S (see Eq. 5) can be calculated from literature absorption cross sections of the target trace gas, a background spectrum $I_0(\lambda)$ and a modeled instrument transfer function (see Sect. 3.1 and 4.2). Alternatively, $\Delta\overline{\sigma}$ can be determined through calibration (see e.g. Lübcke et al., 2013; Sihler et al., 2017).

4 Proof of concept: Field measurements of volcanic SO_2

4.1 Sensitivity and ozone interference

The above model study on trace gas detection with FPI Correlation Spectroscopy was validated in a proof of concept field study for volcanic SO_2. In a one-pixel prototype a single photodiode was used as detector. A BPF ($\lambda_{BPF} \approx 310\,\mathrm{nm}, \delta_{\lambda,BPF} \approx 10\,\mathrm{nm}$) was used for the preselection of a wavelength range, where the SO_2 differential absorption is strong and approximately periodic (see Fig. 2). A FPI (air-spaced etalon from *SLS Optics Ltd.*) with a FSR of $2.1\,\mathrm{nm}$ and a Finesse of 7 across a clear aperture of $20\,\mathrm{mm}$ was tilted by a servo motor in order to tune it to the on-band and off-band transmission settings. The individual plates of the FPI have a finite thickness and two surfaces, the outer surfaces have an anti-reflective coating and are slightly wedged from the inner surfaces of the plates, so their influence can be neglected here. The optical setup behind FPI and BPF consists of a fused silica lens ($f \approx 50\,\mathrm{mm}$), which projects light from a narrow FOV ($\sim 0.8°$ aperture angle) onto the photodiode.

Radiances for the on-band and off-band channel were recorded, delivering an apparent absorbance measurement with $0.42\,\mathrm{Hz}$.

A telescope ($\sim 0.5°$ aperture angle) was co-aligned with the one pixel FPI setup and connected to a temperature stabilized spectrometer (spectral resolution $\sim 0.8\,\mathrm{nm}$). The recorded spectra ($\sim 0.13\,\mathrm{Hz}$) were evaluated with the DOAS algorithm.

The measurement was performed at the *Osservatorio Vulcanologico Pizzi Deneri* (37.766° N, 15.017° E, 2800 m a.s.l.) at Mt. Etna on Sicily on 30 July 2017. The device was pointed towards the volcanic plume of Mt. Etna with constant viewing angle (8° viewing elevation, azimuth 280° N). A plume free part of the sky (zenith viewing direction) was used for reference measurements and recorded prior to the plume measurement. Fig. 6 shows the time series of the apparent absorbance of the FPI Correlation Spectroscopy prototype together with the SO_2 CD retrieved from the co-recorded spectra. The apparent absorbance shows high correlation with the retrieved SO_2 CD. In Fig. 7 the correlation plot is shown. For high SO_2 CDs the sensitivity of $\tilde{\tau}_{SO_2}$ decreases slightly due to saturation effects. The scatter of the values mainly originates from slight misalignment and the difference of the two narrow FOVs.

The recorded UV spectra also allow for evaluating the O_3 absorption. The lower panel of Fig. 6 shows the change of the differential O_3 CD during the measurement with respect to the reference. The observed increase of the O_3 CD by more than $4 \cdot 10^{18}\,\mathrm{molec\,cm^{-2}}$ during the plume measurement is due to the increasing stratospheric light path with increasing solar zenith angle (63.58° to 79.31° during the measurement sequence). Within an imaging FOV (of e.g. 17°) much lower differential O_3 CDs are expected (see Tab. 2), since all pixels are similarly affected by the change in O_3 background. Even with this extreme change in O_3 CD no impact on the recorded SO_2 apparent absorbances is observed.

The presented data also indicates the potential of using an additional DOAS measurement for the calibration of the apparent absorbance of an FPI imaging device. The position of the narrow FOV of a DOAS telescope pointing into the wide imaging FOV can be retrieved from time series and used for an in-operation calibration (see e.g. Lübcke et al., 2013; Sihler et al., 2017).

4.2 Calculation of SO_2 CDs by modeling effective absorption cross sections

As stated in Sect 2.2 we can also directly calculate the SO_2 CDs from the apparent absorbance $\tilde{\tau}$ by modeling the effective absorption cross sections and thereby $\Delta\overline{\sigma}_{\mathrm{SO_2}}$. This requires knowledge about the instrument spectral transmission, the background scattered light spectrum and the SO_2 absorption cross section.

We modeled the instrument transfer function with the transmission spectrum of the used band pass filter, the calculated FPI transmission spectrum (see Sect. 3.1) and the quantum efficiency of the photodiode. The background scattered sunlight spectrum was modeled using a high resolution solar atlas spectrum according to Chance and Kurucz (2010), scaled by the wavelength to the fourth power (assuming Rayleigh scattering) and multiplied with the transmission of the total slant atmospheric ozone column. The ozone column was estimated to $2.5 \cdot 10^{19}\,\mathrm{molec\,cm^{-2}}$ using the vertical ozone column (for the measurement day according to satellite measurements, TEMIS database, Veefkind et al., 2006) multiplied with a geometric air mass factor for the average solar zenith angle during the measurement. The SO_2 absorption cross section of Vandaele et al. (2009) was used.

The largest uncertainties are the finesse of the FPI and the modeled background spectrum, where Rayleigh scattering approximation and the assumed ozone column introduce uncertainties. A finesse of about 7 has been reported by the manufacturer for perpendicularly incident radiation. For the instrument model we have to calculate the effective finesse for a divergent light ray

($\sim 0.8^\circ$ aperture angle) for the two FPI tilt positions (around 0° for setting B and 5° for setting A, corresponding to a finesse of around 7 and 5, respectively). Since the divergent light ray reaching the detector is dependent on focal length, detector area, the alignment of the optical components and due to the uncertainty in the reflectance of the FPI we can determine the finesse only with an uncertainty of $\pm 3\%$. Further we estimate an uncertainty in the background spectrum by $\pm 10\%$ in our calculation, accounting for uncertainties in atmospheric radiative transfer and ozone column.

Figure 8 shows the SO_2 CDs calculated with the described FPI model as a function of the SO_2 CDs retrieved from the DOAS spectra. We observe an excellent agreement with a slope of 0.99, an intercept of $7.5 \cdot 10^{15}\,\mathrm{molec\,cm^{-2}}$ and $R^2 = 0.96$. The uncertainties in background spectral radiance and finesse result in a uncertainty in the SO_2 sensitivity $\Delta\sigma_{SO_2}$ of around $\pm 10\%$ and therefore a relative uncertainty of $\pm 10\%$ in the retrieved SO_2 CD. Here, it is important to highlight the difference between ozone interference with the apparent absorbance and the influence of an uncertainty in the total ozone column assumed in the model. The former seems to be negligible as shown by the measurements (Fig. 6) and in the model study (Sect. 3.2). The latter influences the modeled sensitivity of the measurement. This means, it introduces a small relative uncertainty to the retrieved CDs, which has almost no influence on the detection limit. The saturation effects observed for high CDs in the apparent absorbances (see Fig. 7), meaning the CD dependency of $\Delta\sigma_{SO_2}$, are accounted for by model as well. This is a very promising result, pointing towards the possibility of calibration free measurements, which would be another major advantage of the FPI Correlation Spectroscopy compared to e.g. filter based SO_2 cameras.

4.3 Imaging

The one pixel FPI Correlation Spectroscopy prototype, introduced in this study, can be implemented in a full frame imaging instrument. This is the major advantage of the technique compared with the DOAS technique. The imaging implementation can be achieved with e.g. the image space telecentric optical setup, used for the above calculations and shown in Fig. 5. In principle, the single pixel detector (photodiode) is replaced by a two dimensional detector array (UV sensitive for SO_2 and BrO) and an aperture stop is added in the focal plane in front of the lens. This would, however, reduce the light throughput per pixel of the imaging setup compared to the one pixel prototype. Alternatively, the FPI could be placed in front of the lens using the full clear aperture and the full aperture angle of the FPI and the optics, increasing the light throughput by a factor of 32 (see Kuhn et al., 2014). This leads to a much higher light throughput, however, the incidence angle of the incident light onto the FPI and thereby the FPI transmission spectrum becomes dependent on the pixel (i.e. the viewing direction within the imaging FOV) and has to be accounted for in the data evaluation.

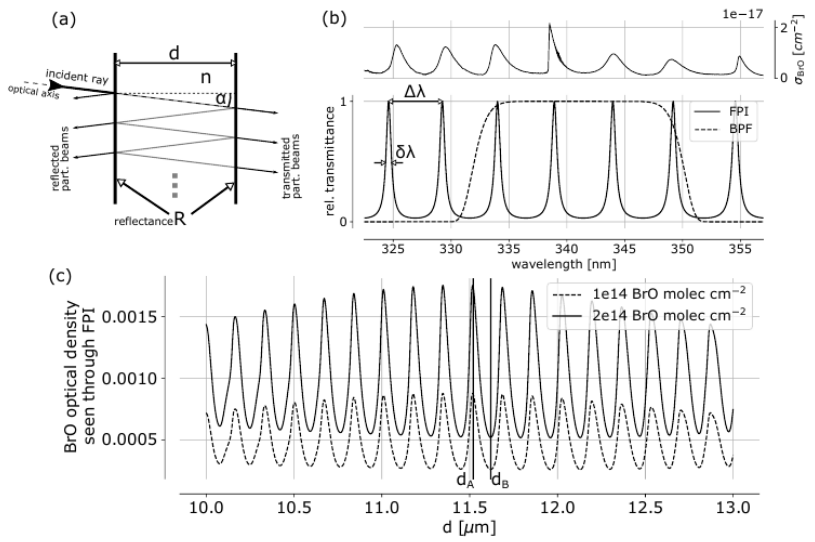

Figure 1. (a) FPI schematics indicating the splitting of incident radiation into partial beams that interfere to cause the FPI transmittance spectrum (b), which is characterised by periodic transmission maxima with a FWHM of δ_λ and a FSR of Δ_λ. The BrO absorption cross section (upper panel) shows approximately periodic structures allowing for a high correlation with spectral FPI transmittance. This leads to a modulation of the BrO optical density as seen through the FPI with changing surface displacement d (c). The apparent absorbance is the difference of the optical densities of FPI settings A and B, representing maximum and minimum correlation of FPI transmission and absorption cross section σ

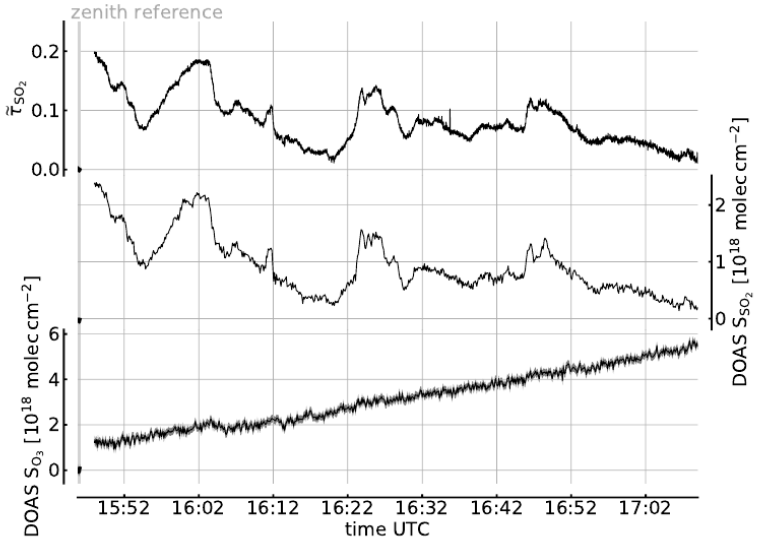

Figure 6. Time series of the apparent absorbance of the one pixel FPI Correlation Spectroscopy prototype for SO_2 detection (top trace, left scale) recorded at Etna, Sicily on 30 July 2017. A co-aligned telescope was used to simultaneously record spectra for DOAS evaluation of SO_2 and O_3 (center and bottom traces and right and bottom left scales, respectively). The apparent absorbance nicely correlates with the SO_2 CD (see Fig. 7), while no O_3 impact is observable. The growth of the retrieved O_3 differential CD is expected due to the increasing stratospheric O_3 column for increasing solar zenith angle (see text).

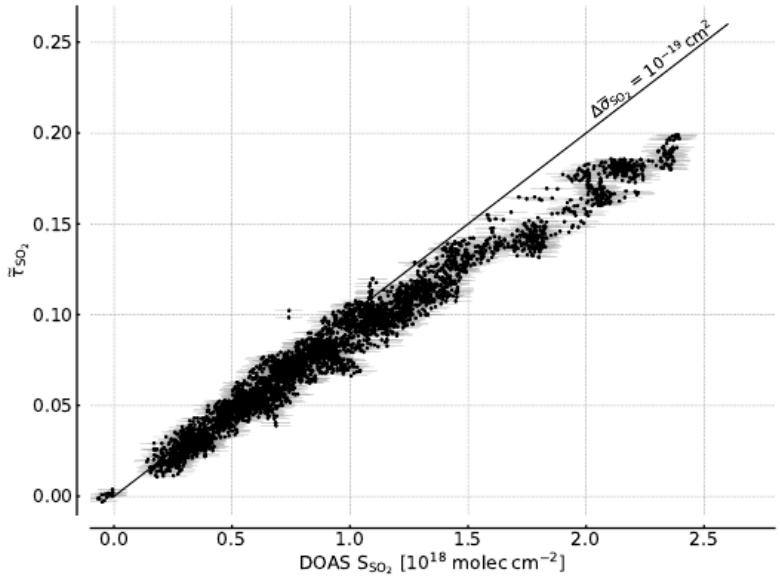

Figure 7. Correlation plot of the recorded FPI Correlation Spectroscopy apparent absorbance and the SO_2 CD retrieved by DOAS. A sensitivity of about $\Delta\bar{\sigma}_{SO_2}$ of 10^{-19} cm^2 is reached for lower SO_2 CDs. For higher CDs a flattening of the curve is observed that is induced by saturation effects due to the high SO_2 optical densities at the absorption peaks.

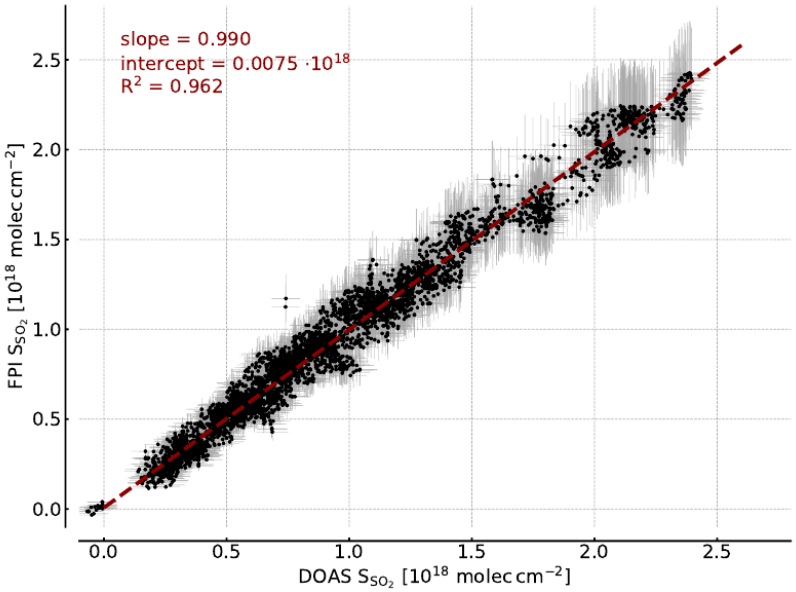

Figure 8. Correlation plot of the SO_2 CDs, retrieved by modeling and the SO_2 CDs retrieved by DOAS. The error bars indicate the uncertainty of the FPI finesse ($\pm 3\%$) and the background spectral radiance in the model ($\pm 10\%$) and the DOAS retrieval error, respectively. A high correlation is observed and even the saturation effects are accounted for by the model, which indicates the potential of calibration free measurements.